Applied Catalysis B: Environmental 187 (2016) 122–133

Contents lists available at ScienceDirect

Applied Catalysis B: Environmental

journal homepage: www.elsevier.com/locate/apcatb

Ti/ZnO–Fe_2O_3 composite: Synthesis, characterization and application as a highly efficient photoelectrocatalyst for methanol from CO_2 reduction

Shengjie Xia [a], Yue Meng [a,b], Xiaobo Zhou [c], Jilong Xue [a], Guoxiang Pan [b], Zheming Ni [a,*]

[a] Department of Chemistry, College of Chemical Engineering, Zhejiang University of Technology, Hangzhou 310032, PR China
[b] Department of Materials Chemistry, School of Life Science, Huzhou Teachers college, Huzhou 313000, PR China
[c] Toxikon Corporation, 15 Wiggins Ave, Bedford, MA 01730, USA

ARTICLE INFO

Article history:
Received 31 October 2015
Received in revised form 6 January 2016
Accepted 11 January 2016
Available online 15 January 2016

Keywords:
Ti/ZnO–Fe_2O_3 composite
Photoelectrocatalysis
Methanol
CO_2 reduction
Mechanism

ABSTRACT

In this paper, Ti/ZnO–Fe_2O_3 composite derived from Ti/Schiff base intercalated ZnFe layered double hydroxides was used as thin film electrode in CO_2 photoelectroreduction. The influence of molar ratio of Ti/Fe and calcination temperature, which would affect the composites' physicochemical property and the photoelectrocatalytic performance for CO_2 reduction, were investigated in detail. The characterization results from XRD, SEM, TEM, UV-vis and BET showed that Ti/ZnO–Fe_2O_3 composite with flower–like crystal from had small particle sizes, narrow band gap and excellent textural properties. The final product of CO_2 photoelectroreduction was methanol and the intermediates were formic acid and formaldehyde. The methanol field reached at 0.773 mmol/cm^2 after 3 h reaction with 0.5 V voltage by Ti/ZnO–Fe_2O_3 composite with Ti/Fe = 1, calcined at 800 °C. In addition, the CO_2 photoelectroreduction pathway and the reason for highly efficient photoelectrocatalytic activity of the composite were also discussed.

1. Introduction

Environmental pollution and greenhouse effect caused by CO_2 has been a practical challenge and drawn widely attention of scientist. At the same time, CO_2 is one of the cheapest compound and the final reaction product for carbon containing compounds; therefore it is the biggest carbon resource in nature. The research and development of CO_2 application is not just a big challenge in the 21st century, but also a great opportunity for economic consideration. The reduction, conversion and application of CO_2 has been the major focus for chemist in the past years, and the effort has generated a great many results for CO_2 elimination [1–5]. The hydrogenation synthesis of methanol is considered as one of the most successful technique among the production of methanol, formaldehyde, methane and dimethyl ether from CO_2, which could relieve the greenhouse effect caused by CO_2 emission [6–8]. Methanol is not only one of the fundamental compound for C–1 chemistry and raw material for organic industry, but also a novel environmental friendly clean power source, it has been generally used in the following areas such as chemical engineering, plastic, dye, synthetic fiber, pesticide, textile and defense industry. The catalysts used in CO_2 hydrogenation includes Cu based catalyst and noble metal supported catalyst. The common disadvantages of these current catalysts are higher energy expenditure, low conversion rate, low selectivity and low productivity [9–12]. Thus the key to improve the photocatalysis process is to find a good performance catalyst for the CO_2 to methanol reaction. Photocatalytic technique with the advantage of high performance and low energy expenditure is the feasible proposal for the resolution of such problem.

As photocatalytic materials, layered double hydroxides (LDHs) have drawn much attention in the environmental waste treatment and energy investigation for its excellent properties [13–17], such as special layered structure, adjustable forbidden band gap, high anion exchange capacity, high light absorption range, easy to be synthesized, low costs and good recyclable properties [18,19]. In addition, the composites of bimetallic or trimetallic oxide could be formed after calcinations. The second or third metals could be highly dispersed and doped into the LDH materials. Thus, the photocatalytic property of these composites could be greatly improved [20,21]. At present, a few researchers have paid attention to the photoreduction of carbon dioxide, but the LDHs materials used in these works were still traditional LDHs or their calcination prod-

* Corresponding author.
E-mail address: jchx@zjut.edu.cn (Z. Ni).

http://dx.doi.org/10.1016/j.apcatb.2016.01.027
0926-3373/

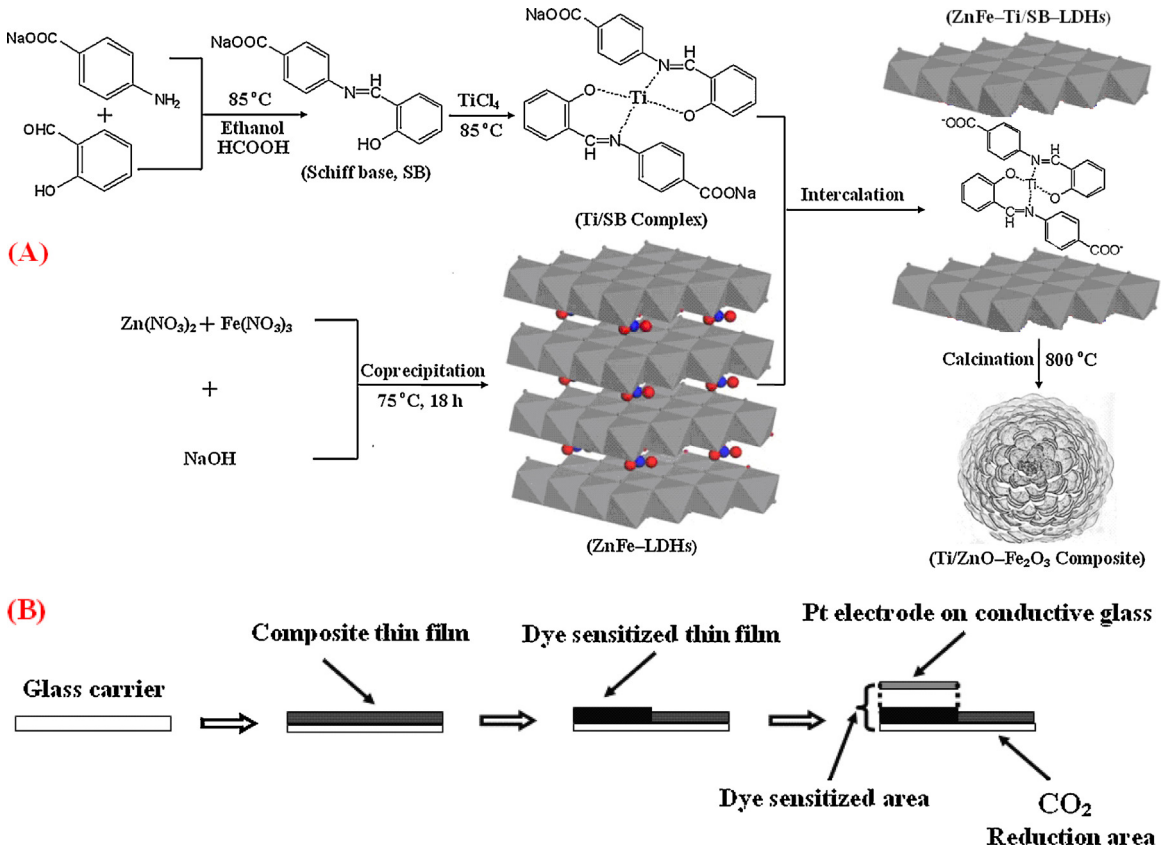

Scheme 1. The preparation pathway for the Ti/ZnO–Fe_2O_3 composite (A) and thin film electrode (B).

ucts [22,23], based on our study, very little progress has been made on the study of Ti–containing LDHs material for CO_2 reduction [24]. Our former research showed that the photocatalytic performance could be improved after the intercalation and calcination of organic ligands contained Ti element into LDHs interlayer [25,26]. Moreover, based on the references [27,28], when an electric field is added to the photocatalytic reaction system, the photoelectrons could be well conducted by the electric field and the combined effect between photocatalysis and electrocatalysis could enhance the catalytic efficiency. In addition, no research has been reported so far on the idea of designing a novel metal oxide composite based on Ti–containing organic–inorganic hybrid material and applying this new material as photoelectrocatalyst for methanol production from CO_2 reduction.

Based on the above–mentioned research idea, Ti–containing schiff base complex was intercalated into the ZnFe–LDHs by ion exchange method, the prepared hybrid LDH material was further calcined at different temperature to obtain the composite of metal oxides (Ti/ZnO–Fe_2O_3 composite). Finally, the Ti/ZnO–Fe_2O_3 composite was dye sensitized and used as thin film electrode. The structural, morphological, textural and semi–conducting properties of those materials were determined by XRD, SEM, TEM, BET, ICP–AES and UV–vis analyses. In addition, the photoelectrocatalytic performance for CO_2 reduction by Ti/ZnO–Fe_2O_3 composite was studied in detail, to understand the influence of synthetic route onto the structure and property of the metal oxides, as well as the reaction mechanism and intermediates for CO_2 reduction under visible light irradiation and voltage. The influence of calcination temperature and molar ratio of Ti/Fe onto the structure and property of the composite was also investigated.

2. Experimental

2.1. Materials

Sodium 4–aminobenzoate and salicylaldehyde were guaranteed reagent (GR) and purchased from Aldrich. Titanium tetrachloride, diethyl ether and formic acid were analytical reagent (AR) and purchased from Aladdin Chemistry Co., Ltd. The others were all purchased from Zhejiang Xiaoshan Fine Chemical Co., Ltd. In addition, deionized water was decarbonated by boiling N_2 before employing in all synthetic process.

2.2. Preparation of photoelectrocatalysts

2.2.1. Synthesis of ZnFe–LDHs

The synthetic procedure of ZnFe–LDHs is given below: an aqueous solution (120 ml) containing 30.0g NaOH (0.75 mol) was added dropwise to a solution (180 ml) contained 66.9 g (0.225 mol) of $Zn(NO_3)_2{\cdot}6H_2O$ and 30.3 g $Fe(NO_3)_3{\cdot}9H_2O$ (0.075 mol) (initial Zn/Fe = 3) with vigorous stirring at 25 °C until the final pH = 8. Then, the resulting slurry was aged at 75 °C for 24 h, centrifuged and washed with deionized water until the pH decreased to 7. Finally it was dried in vacuo at 75 °C for 18 h. After grounded, we could obtain product ZnFe–NO_3–LDHs, which was abbreviated as ZnFe–LDHs.

2.2.2. Preparation of Ti/Schiff–base

First of all, in 250 ml flask, 100 ml of ethanol solution containing 12.24 g (100 mmol) salicylaldehyde was added dropwise into a 80 ml ethanol solution contained 13.72 g (100 mmol) of sodium 4–aminobenzoate and 2 ml of formic acid with vigorous stirring for 30 min. Then, the reaction system was continuously stirred for 3 h at a refluxing temperature of 85 °C. The resultant

slurry was then condensed, refrigerated, filtered, washed with ice–cold ethanol and dissolved with warm ethanol, after repeating the above–mentioned steps three times, finally the product was dried in vacuo oven at 65 °C for 6 h, giving the Schiff–base ligand ($C_{14}H_{10}NO_3Na$, 263 g/mol, abbreviated as SB, the yield = 63.7%, the content of C, H and N: C = 62.43%, H = 3.57%, N = 5.49%).

And then, an ethanolic solution (150 ml) containing as–synthesized Schiff base ligand (10.535 g, 40 mmol) was added dropwise to a solution contained 2.35 ml (20 mmol) of $TiCl_4$ and 50 ml of ethanol with vigorous stirring under the N_2 atmosphere. Then, the produced suspension was stirred for 2 h at a refluxing temperature of 85 °C. The slurry was filtered, washed thrice with ethanol and recrystalized from diethyl ether, finally it was dried in vacuo oven at 65 °C for 6 h, and then we could obtain product of Ti/Schiff–base complex, which was abbreviated as Ti/SB ($((C_{14}H_{10}NO_3Na)_2Ti$, 573.9 g/mol, the yield = 81.8%, the content of C, H, N and Ti: C = 58.17%, H = 3.46%, N = 4.85%, Ti = 8.85%).

2.2.3. Synthesis of Ti/ZnO–Fe_2O_3 composites

Ion–exchange method was used to synthesize ZnFe–Ti/Schiff base–LDHs, the detailed process was given below: firstly, 100 ml of ethanol was added to 2.0 g dried ZnFe–LDHs (4.4 mmol of Fe) and stirred for 1 h; secondly, a designated quality [0.631–3.673 g (1.1–6.4 mmol)] of Ti/Schiff–base complex (the molar ratio of Ti and Fe is from 0.25 to 1.5) was transferred into the above mentioned ethanolic suspension with ZnFe–LDH, and the reaction system was refluxed at 85 °C for 24 h with constant stirring; finally, the product was isolated by filtration, washed with ethanol and kept overnight in vacuum at 65 °C, and then we could obtain the product of ZnFe–Ti/Schiff base–LDHs, which was abbreviated as ZnFe–Ti/SB–LDHs.

2.0 g ZnFe–Ti/SB–LDHs was calcined in a muffle furnace heating in flowing dry air at temperature range of 500–800 °C for 4 h, then grounded, giving the product Ti/ZnO–Fe_2O_3 composite. The preparation pathway for the Ti/ZnO–Fe_2O_3 composite is depicted in Scheme 1(A).

2.2.4. Design of photoelectrocatalytical reactor

Firstly, Ti/ZnO–Fe_2O_3 composite was pasted at the pre–cleaned the glass carrier by tape, the composite layer was scratched even and the layer was kept with the same thickness as the tape. The pasted glass carrier was dried for 30 min under 70 °C in the oven first, and then calcined at 500 °C for 90 min in the furnace.

The second process was dye sensitization and assembly of thin film electrode. The as–prepared thin file electrode was further dye sensitized to improve the catalysis efficiency and visible light utilization rate. The detailed sensitization procedure is: N719 dye was dissolved in anhydrous ethanol in dark room; the composite thin film supported on glass chip was immersed into the N719 solution in a beaker (only half of the thin film was under the liquid surface); the beaker was sealed with plastic film and aluminum foil and storage for 24 h before being dried and used as the thin file electrode material.

The as–prepared thin film was finally assembled as the electrode. To improve the application life, the thin film was assembled as 2 different parts: the dye sensitization part and the catalysis degradation (reduction) part. The following procedure was used for assembly: the assembly film (polytetrafluoroethylene) was attached to the sensitized composite film surface, then the conductive glass supported Pt electrode was attached to the assembly film to form a sandwich structure, this whole set up was heated up to 120 °C for 40 s before cooling back to room temperature. Electrolyte was injected by syringe using vacuum backfilling method. The injection hole was covered by polytetrafluoroethylene and sealed again by heat sealer.

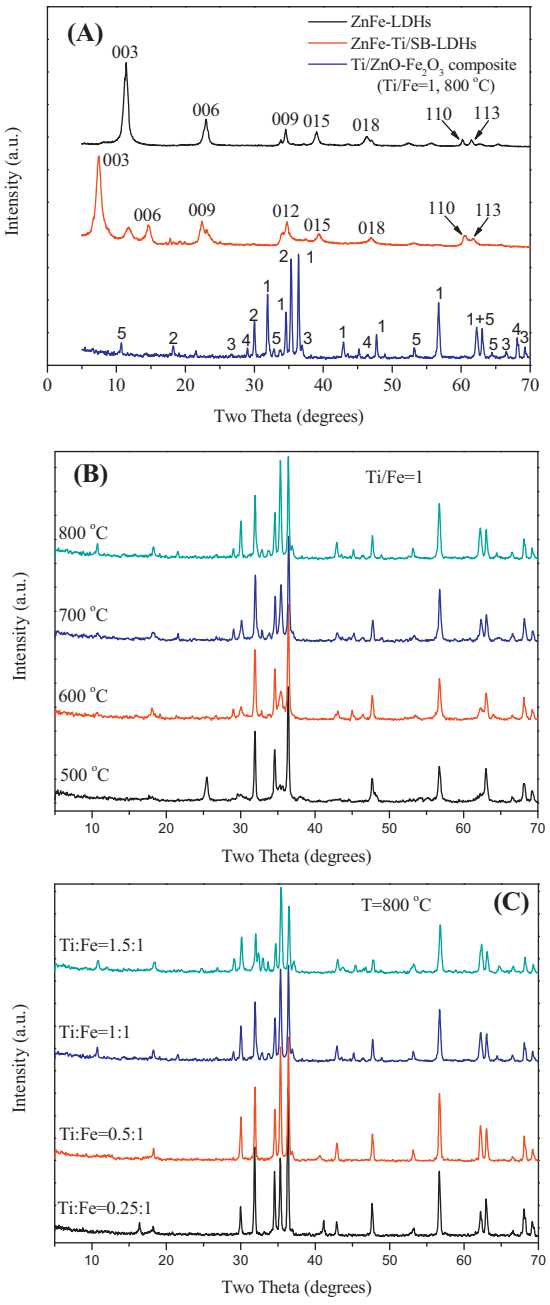

Fig. 1. The XRD patterns for all the samples: (A) contains ZnFe–LDHs, ZnFe–Ti/SB–LDHs and Ti/ZnO–Fe_2O_3 composite calcined at 800 °C; (B) indicates Ti/ZnO–Fe_2O_3 composites calcined at different temperatures (Ti/Fe = 1:1); (C) is Ti/ZnO–Fe_2O_3 composites with different molar ratio of Ti and Fe calcined at 800 °C. Note: (1) ZnO, (2) Fe_2O_3, (3) TiO_2, (4) $ZnFe_2O_4$, (5) $ZnTiO_3$.

The complete preparation pathway for the Ti/ZnO–Fe_2O_3 composite film electrode is depicted in Scheme 1(B).

2.3. Materials characterization

Powder X–ray diffraction (XRD) patterns were recorded on a Rigaku UltimaIV powder diffractometer, using Cu Kα radiation (λ = 1.54 Å) at 40 kV and 178 mA and scanning rate of 5/min in the range of 5–70 . SEM analysis was carried out in a Hitachi SU1510 ESEM with an acceleration voltage of 15 kV. TEM was recorded on a Hitachi HT-7700 to examine the morphologies, lattice fringes and crystal boundaries of the samples. C, H and N elemental microanalyses were obtained on a ThermoFinnigan Italia S.P.A

Table 1
The chemical composition of ZnFe–LDHs and Ti/ZnO–Fe_2O_3 composites.

Samples	Ti/Fe	Calcination (°C)	Zn wt%	Fe wt%	Ti wt%	Chemical formula
ZnFe–LDHs	–	–	38.0	12.1	–	$Zn_{0.73}Fe_{0.27}(OH)_2(NO_3^-)_{0.33}$ $0.43H_2O$
Ti/ZnO–Fe_2O_3	0.25	800	57.2	16.2	3.3	$(ZnO)_{12.56}(Fe_2O_3)_{1.99}(TiO_2)_{0.96}$ $(ZnFe_2O_4)_{0.10}(ZnTiO_3)_{0.04}$
	0.5	800	54.4	15.4	6.2	$(ZnO)_{6.31}(Fe_2O_3)_{0.93}(TiO_2)_{0.94}$ $(ZnFe_2O_4)_{0.14}(ZnTiO_3)_{0.06}$
	1	500	50.9	14.4	9.6	$(ZnO)_{3.82}(Fe_2O_3)_{0.59}(TiO_2)_{0.97}$ $(ZnFe_2O_4)_{0.05}(ZnTiO_3)_{0.03}$
	1	600	50.3	14.3	10.2	$(ZnO)_{3.53}(Fe_2O_3)_{0.53}(TiO_2)_{0.95}$ $(ZnFe_2O_4)_{0.07}(ZnTiO_3)_{0.05}$
	1	700	50.2	14.2	10.3	$(ZnO)_{3.40}(Fe_2O_3)_{0.48}(TiO_2)_{0.92}$ $(ZnFe_2O_4)_{0.11}(ZnTiO_3)_{0.08}$
	1	800	50.2	14.1	10.4	$(ZnO)_{3.33}(Fe_2O_3)_{0.45}(TiO_2)_{0.90}$ $(ZnFe_2O_4)_{0.13}(ZnTiO_3)_{0.10}$
	1.5	800	50.0	14.2	10.4	$(ZnO)_{3.28}(Fe_2O_3)_{0.44}(TiO_2)_{0.89}$ $(ZnFe_2O_4)_{0.14}(ZnTiO_3)_{0.11}$

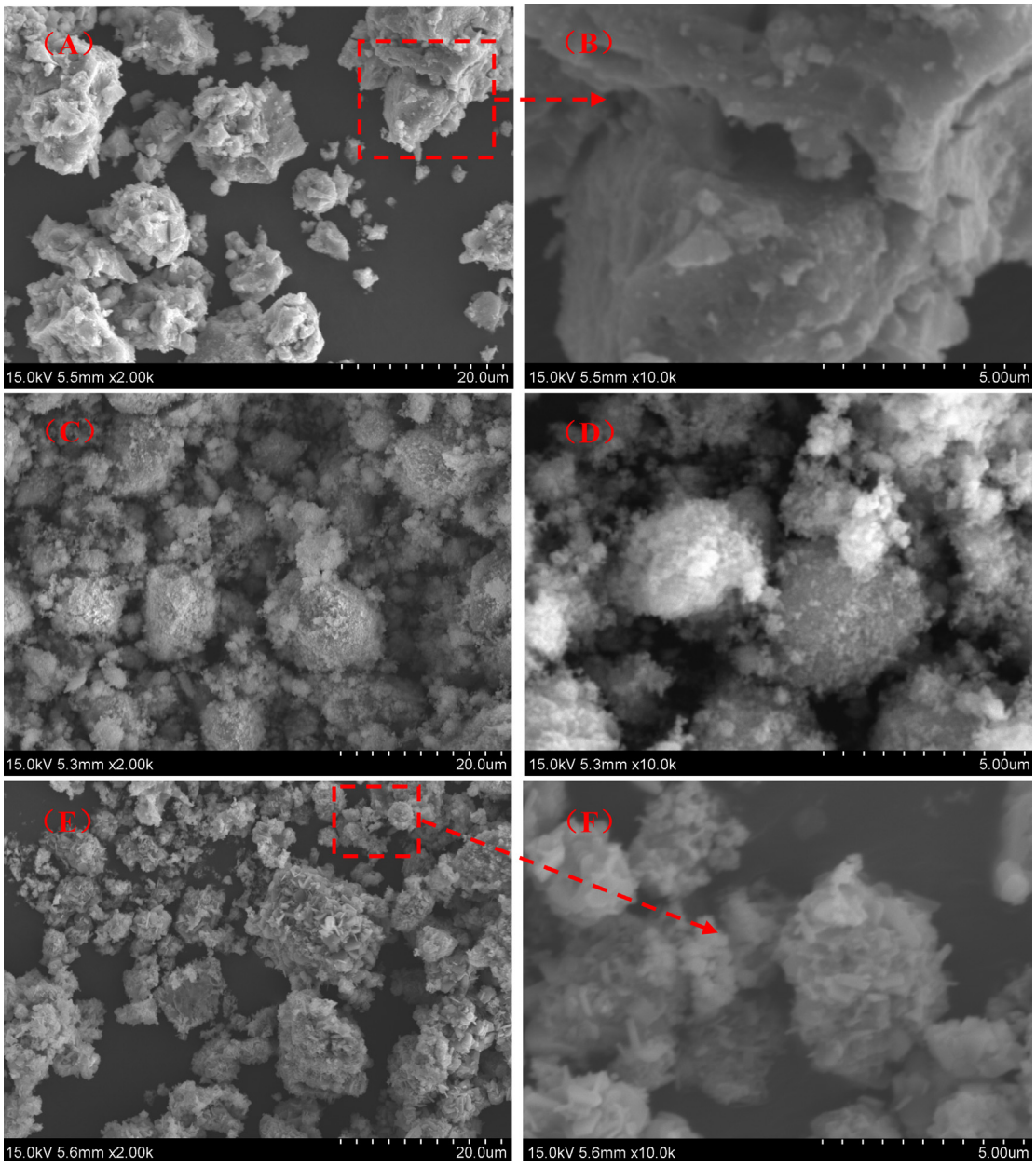

Fig. 2. SEM images for ZnFe–LDHs with low– (A) and high–magnification (B); Ti/ZnO–Fe_2O_3 composite calcined at 500 °C with low- (C) and high-magnification (D); Ti/ZnO–Fe_2O_3 composite calcined at 800 °C with low– (E) and high–magnification (F).

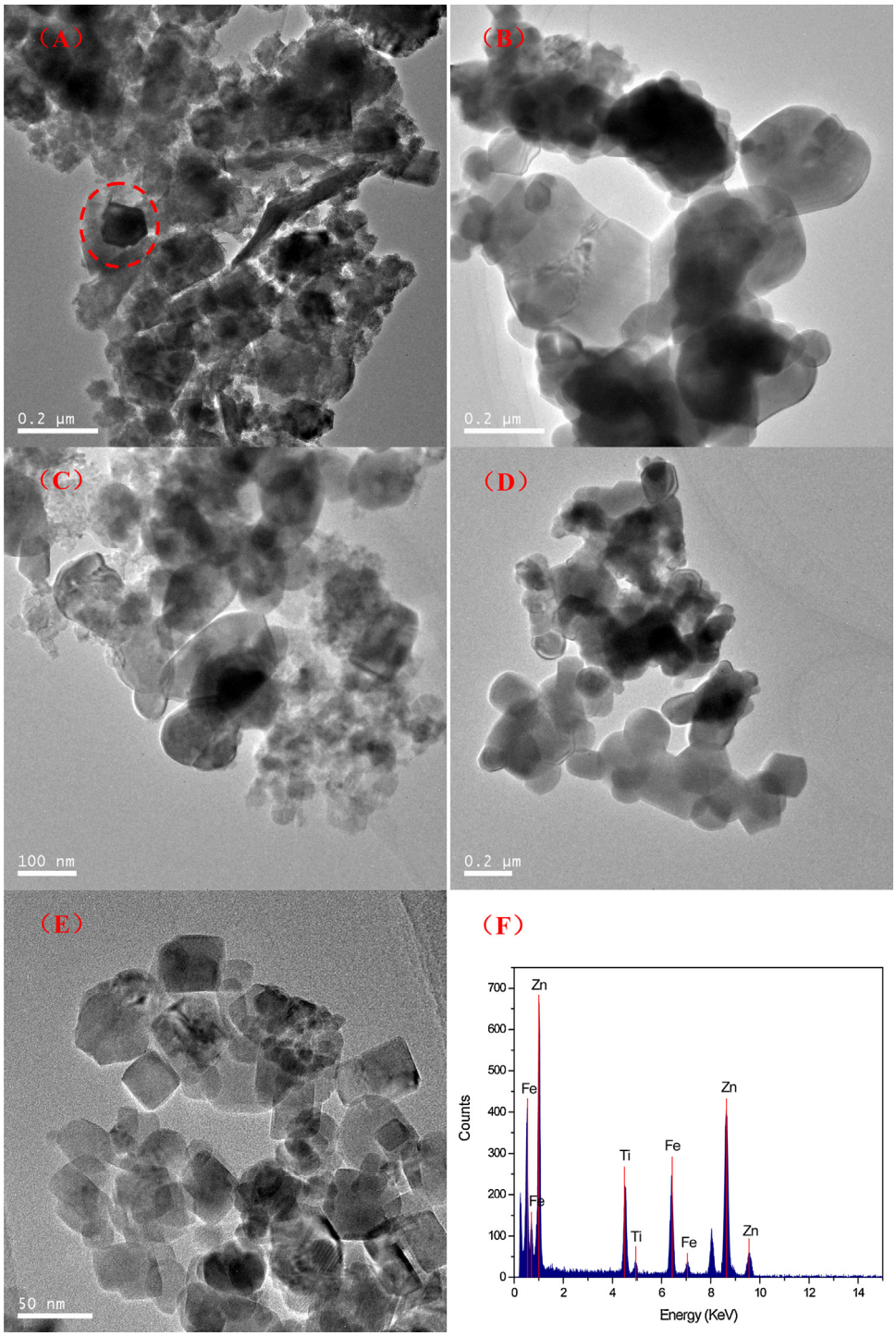

Fig. 3. TEM images for ZnFe–LDHs (A), Ti/ZnO–Fe_2O_3 composite calcined at 500 °C with low– (B) and middle–magnification (C), Ti/ZnO–Fe_2O_3 composite calcined at 800 °C with low- (D) and high-magnification (E), the EDX analysis of designated area (F).

elemental analyzer; Zn, Fe and Ti element analysis were conducted using inductively coupled plasma atomic emission spectrometry (ICP–AES) on a IRIS Intrepid II XSP instrument. The pore structure of the materials was analyzed by N_2 adsorption–desorption at 77 K on a Micromeritics Instrument Corporation ASAP2020 M apparatus. Prior to the analysis, the samples were degassed in a vacuum at 120 °C for 6 h. The specific surface areas were calculated by the Brunauer–Emmett–Teller (BET) method, and the pore size distribution and total pore volume were determined by the Brunauer–Joyner–Hallenda (BJH) method. Solid–state UV–vis diffuse reflectance spectra was recorded at room temperature in air by means of a Shimadzu UV-2550 spectrometer equipped with an integrating sphere attachment using $BaSO_4$ as background.

2.4. Photoelectrocatalytic reaction

The photoelectrocatalytic system was used to study CO_2 reduction. Pt was used as the anode, and Ti/ZnO–Fe_2O_3 composite film electrode was used as the cathode, an electric voltage was applied to the electrodes for the reaction. The film electrode was used for

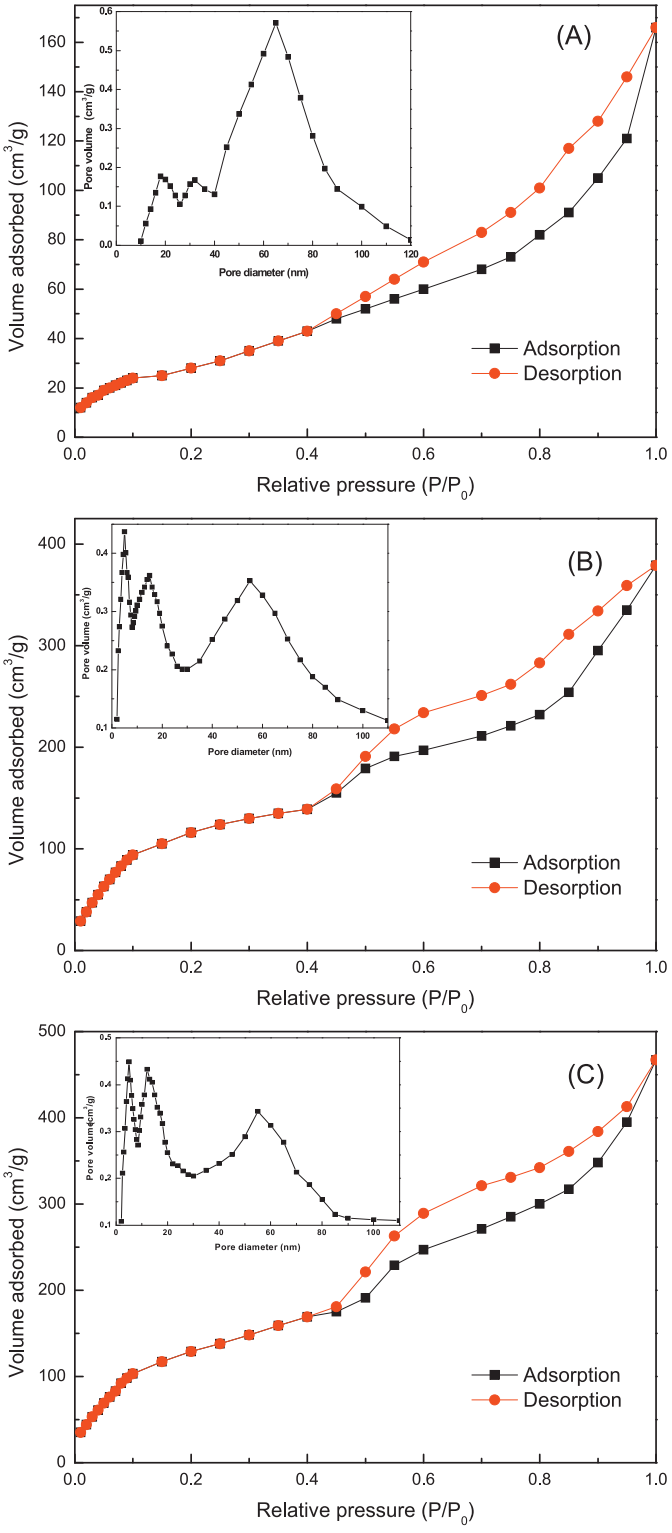

Fig. 4. N_2 sorption isotherms and pore size distribution of ZnFe–LDHs (A), Ti/ZnO–Fe_2O_3 composite with Ti/Fe = 1 and calcined at 500 and 800 °C (B and C).

two functions, the part above the liquid surface was dye sensitized area and exposed to visible light using a 300 W xenon lamp (400 nm < λ < 800 nm) equipped with a constant temperature circulator (15 °C) to generate electrons and holes; the other part was used for the electrocatalytic reduction of CO_2 reduction. During the reaction, the airflow rate of carbon dioxide was 10 m^3/h. The identity and the concentration of reaction intermediates were analyzed

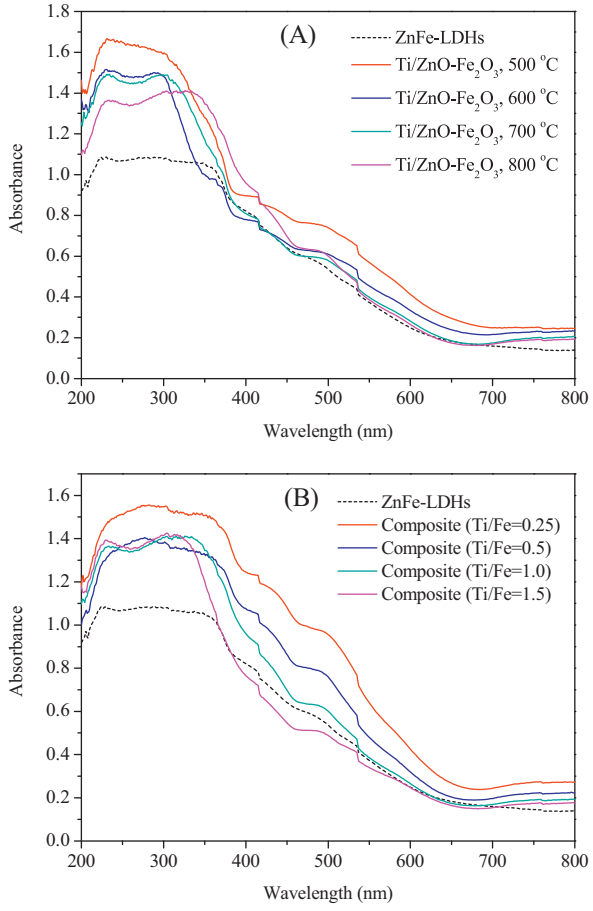

Fig. 5. The UV–vis curves for ZnFe–LDHs and Ti/ZnO–Fe_2O_3 composites: (A) indicates Ti/ZnO–Fe_2O_3 composites (Ti/Fe = 1) calcined at different temperature; (B) is Ti/ZnO–Fe_2O_3 composites with different molar ratio of Ti and Fe calcined at 800 °C.

by GC as well as UV–vis spectrometer (the detailed information is given in Supporting materials). The schematic diagram for photoelectrocatalytical reaction equipment is shown in Fig. S1.

3. Results and discussion

3.1. Structural characteristics of photocatalysts

The XRD patterns for all samples are given in Fig. 1. Fig. 1(A) is the XRD curves of ZnFe–LDHs, ZnFe–Ti/SB–LDHs and Ti/ZnO–Fe_2O_3 composite (Ti/Fe = 1, calcined at 800 °C), from which we could see that the expected peaks of 003, 006, 009, 015, 018 and 110 were all observed in the sample of ZnFe–LDHs and ZnFe–Ti/SB–LDHs, it indicated the successful synthesis of typical LDH materials. Furthermore, the interlayer distance (d_{003}) of ZnFe–LDHs was 0.778 nm (2θ = 11.3 °), it is consisted with the results reported by other authors [29,30]. Particularly for ZnFe–Ti/SB–LDHs, the interlayer distance (d_{003}) of which increased to 1.290 nm (2θ = 6.8 °). The thickness of the LDH layers was 0.48 nm [31], the gallery height of this sample after ion–exchange was 0.81 nm which can be calculated by the interlayer distance minus the thickness of the LDH layers. The increment of gallery height confirmed not only the successful intercalation of the Ti/SB complex, but also the formation of organic–inorganic hybrid material. In addition, as expected, after calcination, the XRD curve of Ti/ZnO–Fe_2O_3 composite showed that the layered structure of original LDHs was completely destroyed and indicated new peaks of metal oxides contained ZnO, Fe_2O_3, TiO_2, and spinel phase of $ZnFe_2O_4$ and $ZnTiO_3$ [32–34].

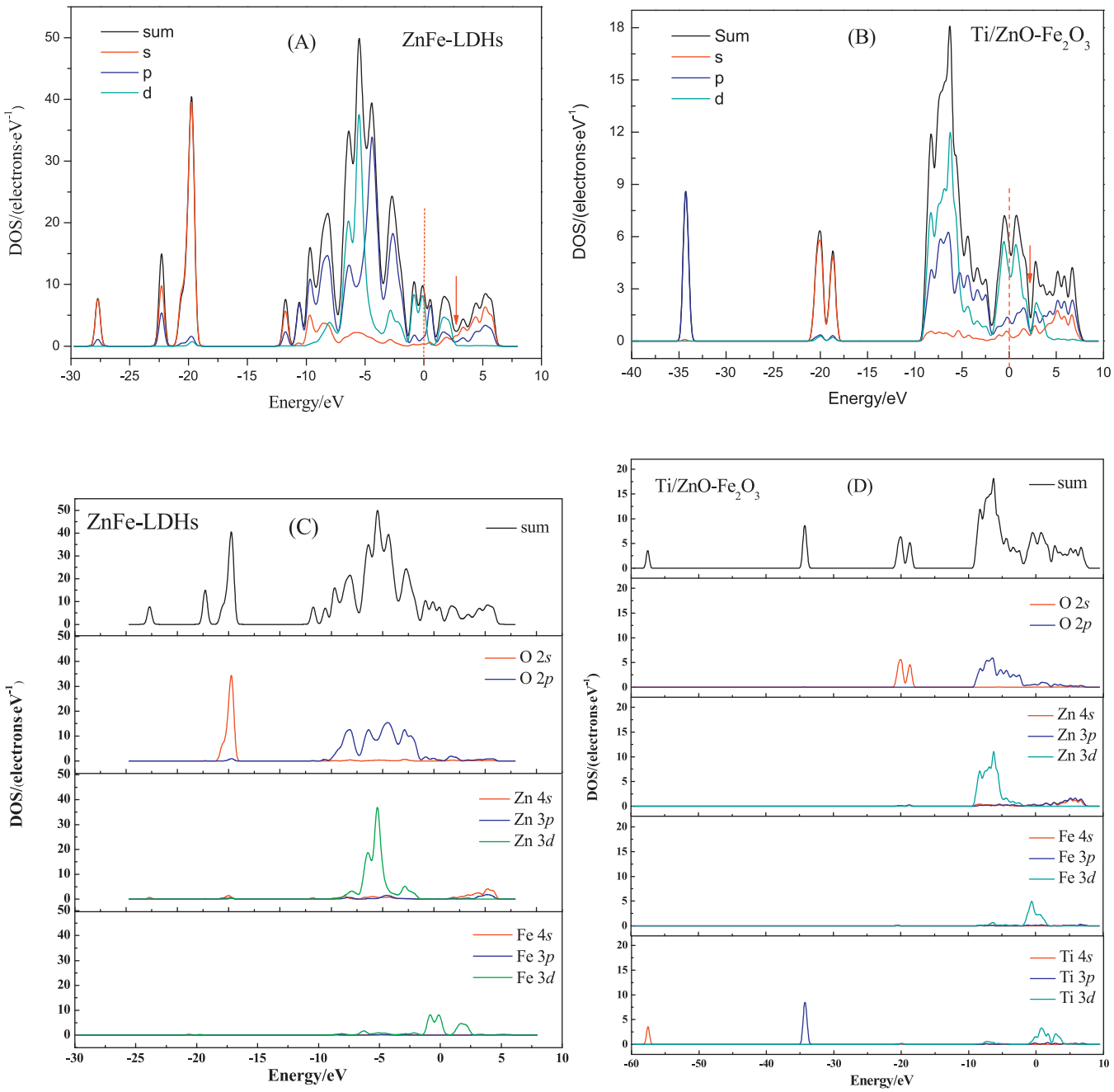

Fig. 6. Total and partial electronic density of states (TDOS and PDOS) (A and B), the electronic density of states of all elements (C and D) for the ZnFe–LDHs and Ti/ZnO–Fe_2O_3 composite with Ti/Fe = 1.

Fig. 1B is the XRD curves for Ti/ZnO–Fe_2O_3 composites with Ti/Fe = 1 and calcined at 500–800 °C. It could be seen that the peaks represent spinel phase of $ZnFe_2O_4$ and $ZnTiO_3$ turned stronger with the increasing of calcination temperature, which could be confirmed by element analysis result (see line 5–8 in Table 1). In addition, the crystal forms of TiO_2 in composites were also changed under the different calcination temperature. When temperature was higher than 700 °C, most of anatase phase of TiO_2 turned to rutile phase. These two structural changes would both benefit to the improvement of photocatalytic activity of Ti/ZnO–Fe_2O_3 composite [35,36]. The XRD patterns of Ti/ZnO–Fe_2O_3 composites with different molar ratio of Ti and Fe calcined at 800 °C is given in Fig. 1C. It indicated that the peaks of TiO_2 and $ZnTiO_3$ turned much shaper with the increasing of Ti/Fe. The XRD curves for the composites with Ti/Fe = 1 and Ti/Fe = 1.5 were quite similar due to the limitation of ion–exchange amount of Ti/SB and nitrate ions of the ZnFe–LDHs, which could be also supported by element analysis result (see lines 8 and 9 in Table 1). Namely, when ZnFe–LDHs was intercalated by Ti/SB complex with equal molar ratio of Ti and Fe, it reached the maximum of ion–exchange amount.

The SEM images for ZnFe–LDHs and Ti/ZnO–Fe_2O_3 composite are shown in Fig. 2. The ZnFe–LDHs sample (Fig. 2A and B) displayed layered lamellar–shape morphology with sharp edges which confirmed the formation of well–ordered LDH materials. Fig. 2C and D is SEM images for Ti/ZnO–Fe_2O_3 composite with Ti/Fe = 1 and calcined at 500 °C, which indicated the formation of irregular–shaped aggregates with grain shape. It showed that after calcination, the original layered morphology LDHs particles converted into mixed metal oxides with irregular morphology stacking particles due to the collapse of layers. While, Fig. 2E and F shows that Ti/ZnO–Fe_2O_3

Table 2
The band gap energy and textural properties of samples.

Catalyst	Ti/Fe	Calcination (°C)	Specific surface area (m^2/g)	Pore size distribution (nm)	Band gap energy (eV)	
					UV–vis	DFT
ZnFe–LDHs	–	–	95	18, 32, 65	2.98	2.79
Ti/ZnO–Fe_2O_3	0.25	800	146	5.0, 12, 55	2.85	–
	0.5	800	155	5.0, 12, 52	2.77	–
	1	500	150	5.0, 15, 55	2.79	2.54
	1	600	159	5.0, 15, 52	2.74	
	1	700	171	5.0, 12, 52	2.67	
	1	800	178	5.0, 12, 50	2.62	
	1.5	800	181	5.0, 12, 50	2.61	

composite calcined at 800 °C had regular flower–shape morphology with agglomerated lamellar crystals onto the composite particles' surfaces. Fig. 3 is the TEM images of ZnFe–LDHs and Ti/ZnO–Fe_2O_3 composite. As shown in Fig. 3A, ZnFe–LDHs nanoparticles displayed obvious and regular layered flake–shape morphology with a crystallite size of 100–150 nm. Fig. 3B and C are Ti/ZnO–Fe_2O_3 composite calcined at 500 °C with low– and middle–magnification, from which we could see that Ti/ZnO–Fe_2O_3 composite calcined at 500 °C showed irregular round plate–shape morphology with a crystallite size about 50–200 nm. It could be seen from Fig. 3D and E, Ti/ZnO–Fe_2O_3 composite calcined at 800 °C showed a cluster constitutes with regular rectangular shape lamellar crystals. The average diameter of those lamellar crystals was about 25–50 nm. Thus, it is obvious that Ti/ZnO–Fe_2O_3 composite calcined at 800 °C not only had smaller particle size, but also showed regular geometry of lamellar crystals than that of composite obtained from 500 °C. In addition, the result of EDS analysis (Fig. 3F) showed that main content of the composite was Zn, Fe and Ti elements.

The N_2 adsorption–desorption isotherm at 77 K and the corresponding pore size distribution curves for ZnFe–LDHs and Ti/ZnO–Fe_2O_3 composite are shown in Fig. 4. Fig. 4A is the isotherm of ZnFe–LDHs, it indicated the presence of mesopores in ZnFe–LDHs due to the type II isotherm with a broad H3 type hysteresis loop ($P/P_0 < 0.4$). Moreover, any limiting adsorption at higher P/P_0 was not observed, indicating the existence of macropores [37], which could be confirmed by the corresponding wide distribution of pore size in Fig. 4A insert. The specific surface area and pore size maximum of ZnFe–LDHs were 95 m^2/g and at 18 nm, 32 nm and 65 nm. In addition, both of the isotherms for Ti/ZnO–Fe_2O_3 composite calcined at 500 °C and 800 °C were type IV (Fig. 4B and C), which was assigned to mesoporous structure, according to the IUPAC classification. Hysteresis loops were belonged to type H3, which were commonly attributed to slit–shaped pores generated by the aggregation of particles [38]. Isotherms for composites calcined at different temperature were somewhat similar, however, there were significant differences in specific surface area, pore volume and pore size distribution. Ti/ZnO–Fe_2O_3 composite obtained at 800 °C showed larger surface area (178 m^2/g) and narrower pore size distribution (pore size maximum at 5.0 nm, 12 nm and 50 nm) than that of composite calcined at 500 °C. The textural properties of Ti/ZnO–Fe_2O_3 composite with different Ti/Fe and calcinations are given in Table 2. It was obvious that Ti/ZnO–Fe_2O_3 composite with high Ti/Fe and obtained from high temperature showed much more excellent physicochemical property than that of other samples.

Fig. 5 shows the UV–vis curves for all the ZnFe–LDHs and Ti/ZnO–Fe_2O_3 composites. It indicated that all of the samples had obvious absorptions at visible light range and Ti/ZnO–Fe_2O_3 composites showed much stronger absorptions than that of ZnFe–LDHs. In addition, the optical band gap energies of the materials were calculated using the formula $Eg = 1240/\lambda$ (λ was the wavelength corresponding to the absorption onset), and also shown in Table 2. The band gap of ZnFe–LDHs was about 2.98 eV, while, after intercalation and calcination, Ti/ZnO–Fe_2O_3 composites showed narrower band gap than that of ZnFe–LDHs. With the increasing of calcination temperature, the ban gap of the composites showed the narrower tendency, from 2.79 to 2.62 eV for 500 °C to 800 °C. In addition, the band gap of composite with different moral ratios was 2.85, 2.77, 2.62 and 2.61 eV for Ti/Fe = 0.25, 0.5, 1 and 1.5, respectively. It implies that the Ti/ZnO–Fe_2O_3 composites with high Ti/Fe and calcination temperature may have highly efficient utilization ratio of visible light than other samples.

Periodic density functional theory (DFT) calculation was used to illustrate the total and partial electronic density of states (TDOS and PDOS) of semiconductors for the purpose of better understanding the electronic band structure of both ZnFe–LDHs and Ti/ZnO–Fe_2O_3 composite (Ti/Fe = 1) [39,40]. The model and structural schematic diagram for ZnFe–LDHs and Ti/ZnO–Fe_2O_3 composite are given in Fig. S2 in Supporting material. The calculating result is shown in Fig. 6 and Table 2. It indicated that the calculated band gap of ZnFe–LDHs and Ti/ZnO–Fe_2O_3 composite was 2.79 eV and 2.54 eV, respectively. The calculation result was in good agreement with the experimental results from UV–vis (see Table 2). In addition, the top of the VB and the bottom of the CB were mainly dominated by the 2s and 2p orbitals of O, 4s of Zn, 3 d of Fe, from the LDH layers contribute to the TDOS of ZnFe–LDHs. While, for Ti/ZnO–Fe_2O_3 composite, 2p orbital of O, 4s and 3p of Zn, 3s and 3p of Fe and 3d of Ti from the metal oxides contributed a lot to the TDOS (Fig. 6C and D).

3.2. The photoelectrocatalytic reduction of carbon dioxide

The GC curve of CO_2 photoelectroreduction products is given in Fig. S3 (Ti/ZnO–Fe_2O_3 composite with Ti/Fe = 1, calcined at 800 °C was used as photoelectrocatalyst). It indicated that the major products were formic acid (retention time was 10.25), formaldehyde (retention time was 1.72) and methanol (retention time was 1.24). In addition, the yield of these three intermediates was calculated by standard lines based on given concentration versus peak area of the samples (see Fig. S4–6 in Supporting materials). Fig. 7A is the concentration changes of formic acid, formaldehyde and methanol during the photoelectrocatalytic reaction. First of all, under dark condition, there was no formic acid, formaldehyde and methanol produced, which indicated that CO_2 photoelectroreduction was powered by light (curves *a*, *b* and *c* in Fig. 7A). Secondly, when light exposure was introduced, after three hours, the concentration for formic acid, formaldehyde and methanol reached at 0.382 mmol/cm^2, 0.529 mmol/cm^2 and 0.327 mmol/cm^2, respectively (curves *d*, *e* and *f* in Fig. 7A). The field was obviously increased but not very high. Finally, when an electric field with 0.3 V was applied into the CO_2 photoelectroreduction, the yield of formic acid, formaldehyde and methanol was greatly increased. After 180 min reaction, the concentrations were 0.685 mmol/cm^2, 0.898 mmol/cm^2 and 0.536 mmol/cm^2, respectively, for these three compounds (curves *g*, *h* and *i* in Fig. 7A). It was obvious that the

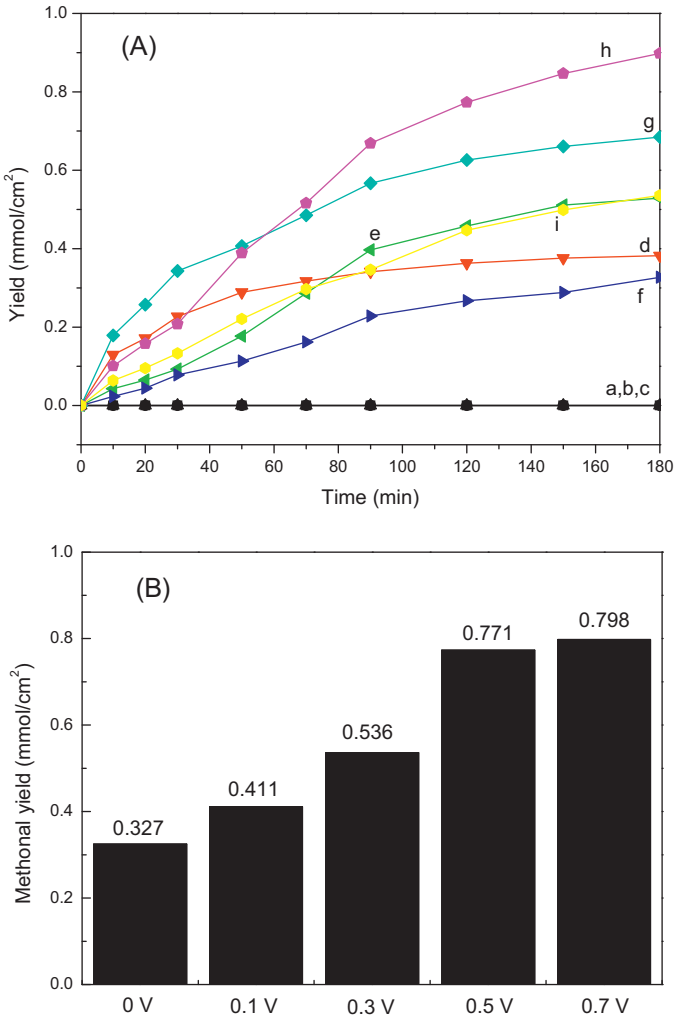

Fig. 7. The concentration change of three products (A) and the effect of external voltage on the yield of methanol (B).
Note: curves of *a*, *b* and *c* are formic acid, formaldehyde and methanol without light; *d*, *e* and *f* are formic acid, formaldehyde and methanol activated by visible light only; *g*, *h* and *i* are formic acid, formaldehyde and methanol which were activated by light and 0.3 V voltage; Ti/ZnO–Fe_2O_3 composite with Ti/Fe = 1, calcined at 800 °C was used as photoelectrocatalyst.

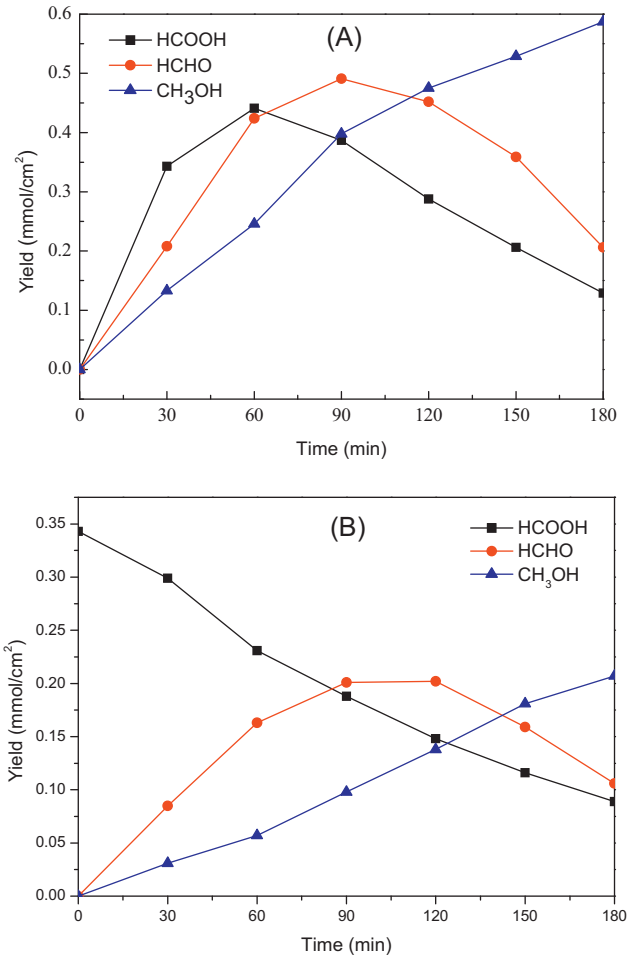

Fig. 8. Yields of CO_2 reduction products: (A) CO_2 supply was stopped after the reaction was run for 60 min; (B) just introduced the same amount of formic acid as the production in the 1st hour in the first experiment group. Note: Ti/ZnO–Fe_2O_3 composite with Ti/Fe = 1, calcined at 800 °C was used as photoelectrocatalyst.

additional electric voltage could further advance the CO_2 reduction efficiency during the photoreaction.

Fig. 7B is the methanol field of CO_2 photoelectroreduction in the condition of different external voltage. It is indicated that the methanol field was dramatically enhanced with the increasing of additional voltage. The methanol field was 0.327 mmol/cm^2, 0.411 mmol/cm^2, 0.536 mmol/cm^2 and 0.773 mmol/cm^2 for 0 V, 0.1 V, 0.3 V and 0.5 V supplied, respectively. While, further increasing the voltage of the photoelectrocatalysis resulted in little increment for methanol field.

3.3. Mechanism for carbon dioxide photoelectroreduction

We designed two groups of experiment to study the formation of those three compounds. In the first group, CO_2 was introduced in the 1st hour of the reaction and shut off in the following two hours. As Fig. 8A shows, after the 1st hour and shut down of CO_2, the formic acid production turned to decline instead of increase, which implies the generation of formic acid is off without CO_2. At the same time, part of the formic acid converted into formaldehyde which brought the increase of formaldehyde after CO_2 was turned off. The conversion from formaldehyde to methanol caused the production decrease of formaldehyde. At the same time, the concentration of methanol was increasing.

The other group just introduced the same amount of formic acid as the production in the 1st hour in the first experiment group, instead of inducing CO_2. From Fig. 8B, the formic acid production is declining all the time which tells the consumption of it. The formaldehyde concentration started with increase and followed by decrease, which could be caused by the formation of formaldehyde from formic acid in the beginning and followed by the conversion from formaldehyde to methanol. The reaction rate from formaldehyde to methanol was higher than the formaldehyde formation from formic acid which caused the concentration drop of formaldehyde. As formic acid and formaldehyde were both converted to methanol, the methanol concentration was increasing all the time. This experiment showed that CO_2 is not directly converted to methanol; instead it goes through the formation of formic acid and followed by formaldehyde formation before the final product methanol. In addition, higher methanol productivity was obtained by shutting off CO_2 supply after 1 h reaction. It could be caused by the electron enrichment effect which is beneficial for methanol formation reaction after the formic acid reaction was turned off for lacking of CO_2. The conversion from formaldehyde to methanol after 2 h reaction showed the capability of the composite film photo electron catalyst to convert formaldehyde to methanol under the synergistic effect of visible light and electricity.

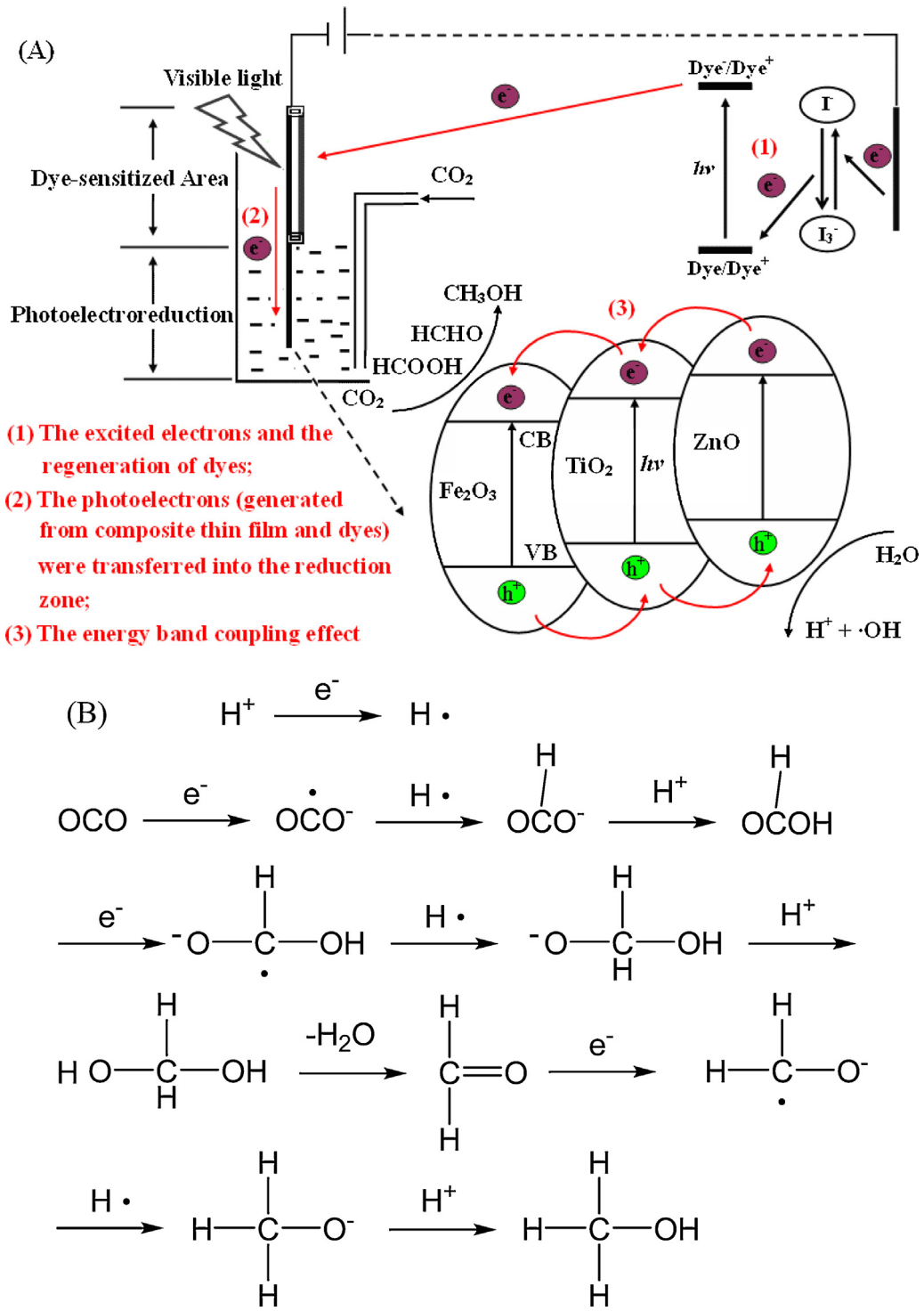

Fig. 9. The schematic diagram of CO_2 reduction mechanism (A) and generation pathway for methanol (B) photoelectrocatalyzed by Ti/ZnO–Fe_2O_3 composite.

Based on the above analysis, we deducted the photo electron reaction mechanism as follows: at the dye sensitization area, the electrons generated from the dye compounds under visible light are transferred to the conductive band of the metal composite and then dispersed. Meanwhile, dye molecules were regenerated and used through the I^-/I_3^- redox pair (Eqs. (1)–(3)). The electric field applied could accelerate the production and transfer of electrons and therefore enhanced the composites' photoelectrorecudtion property. In the photo electron reduction area, the electrons produce $^{\bullet}CO_2^-$ and $^{\bullet}H$ by reaction with the surface absorbed CO_2 and H^+. The $^{\bullet}CO_2^-$ and $^{\bullet}H$ intermediates generate $HCOO^-$, and formic acid and formaldehyde are finally reduced to methanol.

$$3I^- \rightarrow I_3^- + 2e^- \quad (1)$$

$$2dye^+ + 2e^- \rightarrow 2dye \quad (2)$$

$$I_3^- + 2e^- \rightarrow 3I^- \quad (3)$$

As reference reported, when two types of semiconductive materials were recombined, there was energy band coupling effect at the phase surface [41,42]. With light excitation condition, the

electron–hole pairs at the semi conductive material surface could move with the vector direction and avoid the degeneration of electron–hole pair and therefore increase the photo electron catalytic activity. As the conductive band of Fe_2O_3 is lower compared to ZnO and TiO_2, this difference causes the re–distribution of photo generated carrier between three particles: the electrons generated from higher energy band of ZnO will transfer to TiO_2 and Fe_2O_3 bands, the enrichment of electrons at Fe_2O_3 decreases the electron surface density at ZnO and TiO_2; the holes are moved from Fe_2O_3 band to ZnO and TiO_2 conduction bands. The separation of photo generated carriers decrease the degeneration of them and increased its life time, which brings the high catalytic activity of Ti/ZnO–Fe_2O_3 composite to the CO_2 reduction. The schematic diagram of CO_2 reduction mechanism and generation pathway for methanol photocatalyzed by Ti/ZnO–Fe_2O_3 composite is shown in Fig. 9.

In addition, based on the XRD and element analysis characterization results, we known that the content of spinel ($ZnFe_2O_4$ and $ZnTiO_3$) in Ti/ZnO–Fe_2O_3 composite would increase with the enhancement of calcination temperature and Ti/Fe. So, we designed an experiment as a contrast to investigate the influence of spinel into the photoelectrocatalytic performance of composite. The mixture contained the same content of ZnO, Fe_2O_3 and TiO_2 with Ti/ZnO–Fe_2O_3 composite (Ti/Fe = 1, 800 °C) was dye sensitized and used as thin film electrode in the photoelectroreduction of CO_2. The result was given in Fig. S7, after 3 h, the filed of methanol catalyzed by the oxide mixture was only 0.362 mmol/cm^2, which was smaller than half of the methanol filed by the composite. The energy band coupling effect at the phase surface of composite may be strengthened by spinel phase. In that condition, it is more benefit for the movement with the vector direction and existing time of electron–hole pairs at the semiconductive material surface and therefore further increased the photoelectrocatalytic activity.

4. Conclusions

Ti/ZnO–Fe_2O_3 composite was synthesized by calcination of Ti/Schiff base intercalated ZnFe layered double hydroxides (ZnFe–LDHs). The composite was then dye sensitized and used as thin film electrode in the photoelectroreduction of CO_2. The characterization results indicated that Ti/ZnO–Fe_2O_3 composite calcined from layered hybrid material not only showed regular flower–shape morphology, but also had higher specific area, more uniform pores size distribution and narrower band gap than that of ZnFe–LDHs. The ratio of Ti and Fe, calcination temperature could both greatly influence the crystal structure and physicochemical property of Ti/ZnO–Fe_2O_3 composite. When the composite obtained in the condition of Ti/Fe = 1 and 800 °C, it showed the highest specific surface area (178 m^2/g) and narrowest band gap (2.62 eV). Moreover, the electronic band structure of ZnFe–LDHs and composite analyzed by periodic density functional theory (DFT) calculation was in good agreement with the experimental result from UV–vis. The CO_2 photoelectroreduction results showed that Ti/ZnO–Fe_2O_3 composite had excellent performance for methanol from CO_2 reduction activated by both visible light and voltage. The field of methanol from CO_2 reduction by the composite (Ti/Fe = 1, calcinations temperature = 800 °C) reached at 0.771 mmol/cm^2 after180 min of reaction. CO_2 went through the formation of formic acid and followed by formaldehyde formation before the final product methanol. The energy band coupling effect at the phase surface of Ti/ZnO–Fe_2O_3 composite may be the important factor for highly effective photoelectrocatalytic performance of the material. Thus, this research work was designed to contribute to the photoelectrocatalytic mechanism of methanol from CO_2 reduction.

Acknowledgments

This work is supported by National Natural Science Foundation of China (21503188) and Zhejiang Provincial Natural Science Foundation of China (LQ15B030002).

Appendix A. Supplementary data

Supplementary data associated with this article can be found, in the online version, at http://dx.doi.org/10.1016/j.apcatb.2016.01.027.

References

[1] S.D. Sharma, M. Azzi, A critical review of existing strategies for emission control in the monoethanolamine-based carbon capture process and some recommendations for improved strategies, Fuel 121 (2014) 178–188.
[2] J.Q. Torres, S. Royer, J.P. Bellat, J.M. Giraudon, J.F. Lamonier, Formaldehyde: catalytic oxidation as a promising soft way of elimination, ChemSusChem 6 (2013) 578–592.
[3] P. Lanzafame, G. Centi, S. Perathoner, Catalysis for biomass and CO_2 use through solar energy: opening new scenarios for a sustainable and low-carbon chemical production, Chem. Soc. Rev. 43 (2014) 7562–7580.
[4] L.H. Yang, H.M. Wang, Recent advances in carbon dioxide capture, fixation, and activation by using *N*-heterocyclic carbenes, ChemSusChem 7 (2014) 962–998.
[5] N. von der Assen, P. Voll, M. Peters, A. Bardow, Life cycle assessment of CO_2 capture and utilization: a tutorial review, Chem. Soc. Rev. 43 (2014) 7982–7994.
[6] A. Goeppert, M. Czaun, J.P. Jones, G.K.S. Prakash, G.A. Olah, Recycling of carbon dioxide to methanol and derived products-closing the loop, Chem. Soc. Rev. 43 (2014) 7995–8048.
[7] R. Reichert, J. Schnaidt, Z. Jusys, R.J. Behm, The influence of reactive side products on the electrooxidation of methanol-a combined in situ infrared spectroscopy and online mass spectrometry study, Phys. Chem. Chem. Phys. 16 (2014) 13780–13799.
[8] X. Zeng, M. Hatakeyama, K. Ogata, J.K. Liu, Y.Q. Wang, Q. Gao, K. Fujii, M. Fujihira, F.M. Jin, S. Nakamura, New insights into highly efficient reduction of CO_2 to formic acid by using zinc under mild hydrothermal conditions: a joint experimental and theoretical study, Phys. Chem. Chem. Phys. 16 (2014) 19836–19840.
[9] S. Goodarznia, K.J. Smith, The effect of Cu loading on the formation of methyl formate and C–2–oxygenates from CH_3OH and CO over K–or Cs–promoted Cu–MgO catalysts, J. Mol. Catal. A: Chem. 353 (2012) 58–66.
[10] J.A. Rodriguez, J. Evans, L. Feria, A.B. Vidal, P. Liu, K. Nakamura, F. Illas, CO_2 hydrogenation on Au/TiC, Cu/TiC, and Ni/TiC catalysts: production of CO methanol, and methane, J. Catal. 307 (2013) 162–169.
[11] G. Merza, B. Laszlo, A. Oszko, G. Potari, K. Baan, A. Erdohelyi, The direct synthesis of dimethyl carbonate by the oxicarbonylation of methanol over Cu supported on carbon nanotube, J. Mol. Catal. A: Chem. 393 (2014) 117–124.
[12] D.H. Won, C.H. Choi, J. Chung, S.I. Woo, Photoelectrochemical production of formic acid and methanol from carbon dioxide on metal–decorated CuO/Cu_2O–layered thin films under visible light irradiation, Appl. Catal. B 158 (2014) 217–223.
[13] M.Q. Zhao, Q. Zhang, J.Q. Huang, F. Wei, Hierarchical nanocomposites derived from nanocarbons and layered double hydroxides–properties synthesis, and applications, Adv. Funct. Mater. 22 (2012) 675–694.
[14] E. Dvininov, M. Ignat, P. Barvinschi, M.A. Smithers, E. Popovici, New SnO_2/MgAl–layered double hydroxide composites as photocatalysts for cationic dyes bleaching, J. Hazard. Mater. 177 (2010) 150–158.
[15] K. Teramura, S. Iguchi, Y. Mizuno, T. Shishido, T. Tanaka, Photocatalytic conversion of CO_2 in water over layered double hydroxides, Angew. Chem. Int. Ed. 51 (2012) 8008–8011.
[16] T. Nakato, H. Ueda, S. Hashimoto, R. Terao, M. Kameyama, E. Mouri, Pickering emulsions prepared by layered niobate $K_4Nb_6O_{17}$ intercalated with organic cations and photocatalytic dye decomposition in the emulsions, ACS Appl. Mater. Interfaces 4 (2012) 4338–4347.
[17] J.S. Valente, F. Tzompantzi, J. Prince, Highly efficient photocatalytic elimination of phenol and chlorinated phenols by CeO_2/MgAl layered double hydroxides, Appl. Catal. B 102 (2011) 276–285.
[18] M. Gong, Y.G. Li, H.L. Wang, Y.Y. Liang, J.Z. Wu, J.G. Zhou, J. Wang, T. Regier, F. Wei, H.J. Dai, An ddvanced Ni–Fe layered double hydroxide electrocatalyst for water oxidation, J. Am. Chem. Soc. 135 (2013) 8452–8455.
[19] J.L. Gunjakar, T.W. Kim, H.N. Kim, I.Y. Kim, S.J. Hwang, Mesoporous layer-by-layer ordered nanohybrids of layered double hydroxide and layered metal oxide: highly active visible light photocatalysts with improved chemical stability, J. Am. Chem. Soc. 133 (2011) 14998–15007.
[20] Z.J. Huang, P.X. Wu, Y.H. Lu, X.R. Wang, N.W. Zhu, Z. Dang, Enhancement of photocatalytic degradation of dimethyl phthalate with nano–TiO_2 immobilized onto hydrophobic layered double hydroxides: a mechanism study, J. Hazard. Mater. 246–247 (246) (2013) 70––.

[21] D. Carriazo, M. del Arco, E. Garcia-Lopez, G. Marci, C. Martin, L. Palmisano, V. Rives, Zn,Al hydrotalcites calcined at different temperatures: preparation, characterization and photocatalytic activity in gas–solid regime, J. Mol. Catal. A: Chem. 342–43 (2011) 83–90.
[22] E.M. del Campo, J.S. Valente, T. Pavon, R. Romero, A. Mantilla, R. Natividad, 4–Chlorophenol oxidation photocatalyzed by a calcined Mg–Al–Zn layered double hydroxide in a co-current downflow bubble column, Ind. Eng. Chem. Res. 50 (2011) 11544–11552.
[23] A. Mantilla, G. Jacome-Acatitla, G. Morales-Mendoza, F. Tzompantzi, R. Gomez, Photoassisted degradation of 4–chlorophenol and *p*–Cresol using MgAl hydrotalcites, Ind. Eng. Chem. Res. 50 (2011) 2762–2767.
[24] S. Pausova, J. Krysa, J. Jirkovsky, G. Mailhot, V. Prevot, Photocatalytic behavior of nanosized TiO_2 immobilized on layered double hydroxides by delamination/restacking process, Environ. Sci. Pollut. Res. 19 (2012) 3709–3718.
[25] S.J. Xia, F.X. Liu, Z.M. Ni, W. Shi, J.L. Xue, P.P. Qian, Ti–based layered double hydroxides: efficient photocatalysts for azo dyes degradation under visible light, Appl. Catal. B 144 (2014) 570–579.
[26] S.J. Xia, L.Y. Zhang, X.B. Zhou, M.M. Shao, G.X. Pan, Z.M. Ni, Fabrication of highly dispersed Ti/Zn O-Cr_2O_3 composite as highly efficient photocatalyst for naphthalene degradation, Appl. Catal. B 176 (2015) 266–277.
[27] E. Brillas, C.A. Martinez-Huitle, Decontamination of wastewaters containing synthetic organic dyes by electrochemical methods. An updated review, Appl. Catal. B 166 (2015) 603–643.
[28] M. Grzelczak, J.S. Zhang, J. Pfrommer, J. Hartmann, M. Driess, M. Antonietti, X.C. Wang, Electro–and photochemical water oxidation on ligand–free Co_3O_4 nanoparticles with tunable sizes, ACS Catal. 3 (2013) 383–388.
[29] K.M. Parida, L. Mohapatra, Carbonate intercalated Zn/Fe layered double hydroxide: a novel photocatalyst for the enhanced photo degradation of azo dyes, Chem. Eng. J. 179 (2012) 131–139.
[30] Z.P. Liu, R.Z. Ma, Y. Ebina, N. Iyi, K. Takada, T. Sasaki, General synthesis and delamination of highly crystalline transition–metal–bearing layered double hydroxides, Langmuir 23 (2007) 861–867.
[31] Q. Wang, D. O'Hare, Recent advances in the synthesis and application of layered double hydroxide (LDH) nanosheets, Chem. Rev. 112 (2012) 4124–4155.
[32] Y.Z. Wang, S.H. Luo, Z.G. Wang, Y. Fu, Structural and textural evolution of nanocrystalline Mg–Al layered double hydroxides during mechanical treatment, Appl. Clay Sci. 80–81 (2013) 334––.
[33] A. Iwaszuk, M. Nolan, Q.L. Jin, M. Fujishima, H. Tada, Origin of the visible-light response of Nickel(II) oxide cluster surface modified Titanium(IV) dioxide, J. Phys. Chem. C 117 (2013) 2709–2718.
[34] A. Venugopal, R. Sarkari, C. Anjaneyulu, V. Krishna, M.K. Kumar, N. Narender, A.H. Padmasri, Influence of acid–base sites on ZnO–$ZnCr_2O_4$ catalyst during dehydrocyclization of aqueous glycerol and ethylenediamine for the synthesis of 2–methylpyrazine: kinetic and mechanism studies, Appl. Catal. A: Gen. 469 (2014) 398–409.
[35] Y.F. Zhao, P.Y. Chen, B.S. Zhang, D.S. Su, S.T. Zhang, L. Tian, J. Lu, Z.X. Li, X.Z. Cao, B.Y. Wang, M. Wei, D.G. Evans, X. Duan, Highly dispersed TiO6 units in a layered double hydroxide for water splitting, Chem. Eur. J. 18 (2012) 11949–11958.
[36] C. Alanis, R. Natividad, C. Barrera-Diaz, V. Martinez-Miranda, J. Prince, J.S. Valente, Photocatalytically enhanced Cr(VI) removal by mixed oxides derived from MeAl (Me:Mg and/or Zn) layered double hydroxides, Appl. Catal. B 140 (2013) 546–551.
[37] J. Yu, S. Liu, H. Yu, Microstructures and photoactivity of mesoporous anatase hollow microspheres fabricated by fluoride-mediated self-transformation, J. Catal. 249 (2007) 59–66.
[38] J. Tang, Z. Zou, J. Ye, Efficient photocatalysis on $BaBiO_3$ driven by visible light, J. Phys. Chem. C 111 (2007) 12779–12785.
[39] I.M. Nangoi, V.S. Vaiss, W.F. Souza, S.S.X. Chiaro, A.A. Leitao, Theoretical studies of the interaction of terephthalate anion in MgAl-layered double hydroxides, Appl. Clay Sci. 107 (2015) 131–137.
[40] X. Liu, X.F. Zhao, Y. Zhu, F.Z. Zhang, Experimental and theoretical investigation into the elimination of organic pollutants from solution by layered double hydroxides, Appl. Catal. B 140 (2013) 241–248.
[41] L.R. Zheng, Y.H. Zheng, C.Q. Chen, Y.Y. Zhan, X.Y. Lin, Q. Zheng, K.M. Wei, J.F. Zhu, Inorg. Chem 48 (*2009*) 1819–1825.
[42] Z.Y. Wang, B.B. Huang, Y. Dai, X.Y. Qin, X.Y. Zhang, P. Wang, H.X. Liu, J.X. Yu, J. Phys. Chem. C 113 (2009) 4612–4617.